Supplementary Information

RNase H2 disordered region is a DNA mechanosensor in 1D and 3D search of ribonucleotides

Yi Zhao[1,8], Yuting Zhang[1,8], Xinyang Chen[2,8], Yihan Wu[2], Yanan Li[1,3], Zhiyun Ren[1,4,5], Bingkai Cheng[1], Meng Hu[1], Xiaoxuan Song[1], Lishuang Chen[1], Cong Liu[6], Chao Liu[7], Wei Li[7], Zhonghuai Hou[2]✉, & Bo Sun[1]✉

[1]School of Life Science and Technology, ShanghaiTech University, Shanghai, China. [2]Hefei National Research Center for Physical Sciences at the Microscale & Department of Chemical Physics, University of Science and Technology of China, Hefei, China. [3]College of Life Sciences, Xinyang Normal University, Xinyang, China. [4]CAS Center for Excellence in Molecular Cell Science, Shanghai Institute of Biochemistry and Cell Biology, Chinese Academy of Sciences, Shanghai, China. [5]University of Chinese Academy of Sciences, Beijing, China. [6]Interdisciplinary Research Center on Biology and Chemistry, State Key Laboratory of Chemical Biology, Shanghai Academy of Natural Sciences (SANS), Shanghai Institute of Organic Chemistry, Chinese Academy of Sciences, Shanghai, China. [7]Guangzhou Women and Children's Medical Center, Guangzhou Medical University, Guangzhou, China. [8]These authors contributed equally: Yi Zhao, Yuting Zhang, Xinyang Chen.

✉e-mail: hzhlj@ustc.edu.cn; sunbo@shanghaitech.edu.cn

This file includes

Supplementary Figures S1 – S17

Supplementary Table S1

Supplementary References S1 – S3

Supplementary Figures

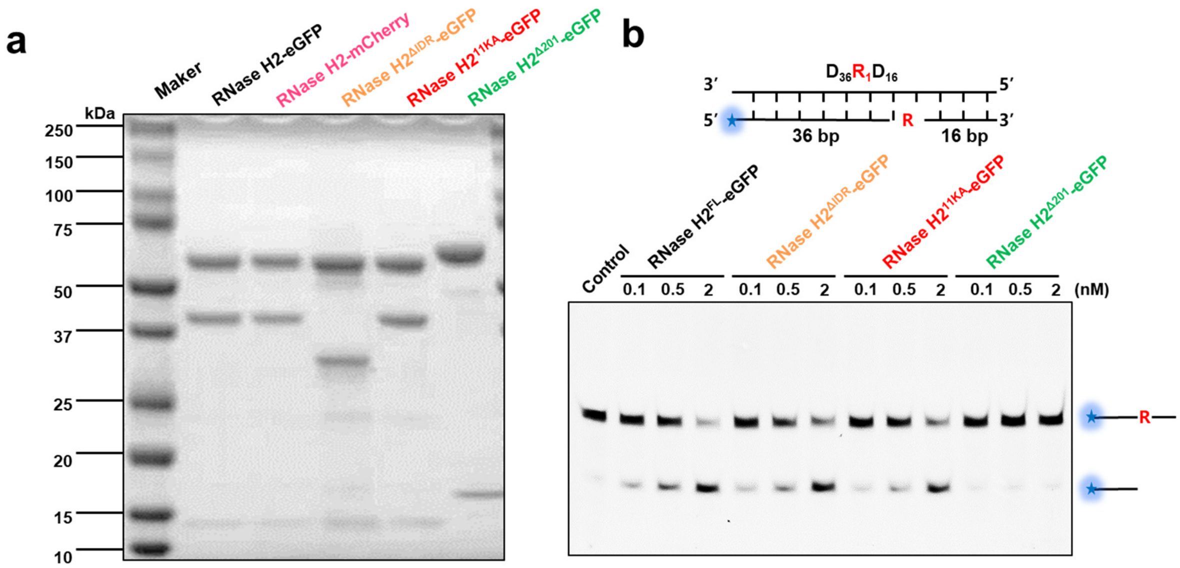

Figure S1. Examining the nuclease activity of fluorescently labeled RNase H2 variants. (a) The representative gels of purified recombinant RNase H2-eGFP, RNase H2-mCherry, RNase H2$^{\Delta IDR}$-eGFP, RNase H2^{11KA}-eGFP, and RNase H2$^{\Delta 201}$-eGFP proteins. **(b)** A representative gel image showing cleavage of RDR/D substratesby RNase H2 variants. Specifically, 0.1 nM, 0.5 nM, and 2 nM RNase H2 variants were incubated with 10 nM of the 53 bp RDR/D substrates (**Table S1**) in the cleavage buffer (25 mM Tris-HCl pH 8.0, 50 mM KCl, 10 mM $MgCl_2$, 0.1 mg/mL BSA, 1 mM DTT) at 25 °C for 10 minutes. The reactions were terminated by adding formamide gel loading buffer supplemented with 20 mM EDTA, followed by heating at 95 °C for 10 minutes.

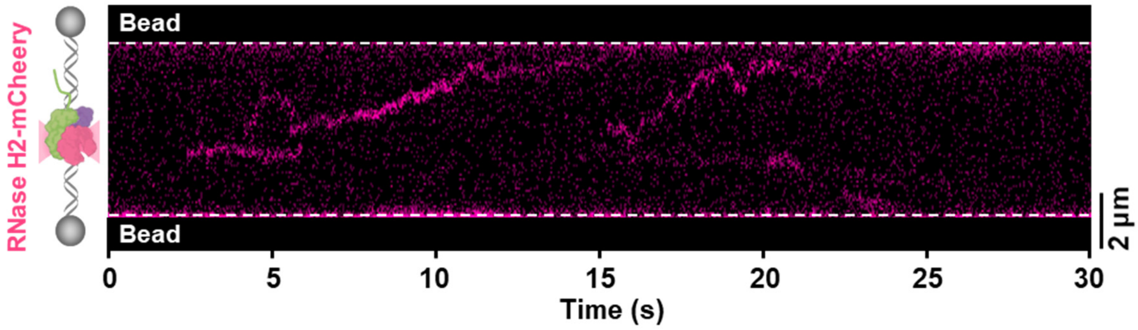

Figure S2. RNase H2-mCherry diffuses along dsDNA. A representative kymograph showing the 1D diffusion of RNase H2-mCherry (200 pM) on a single DNA under 10 pN.

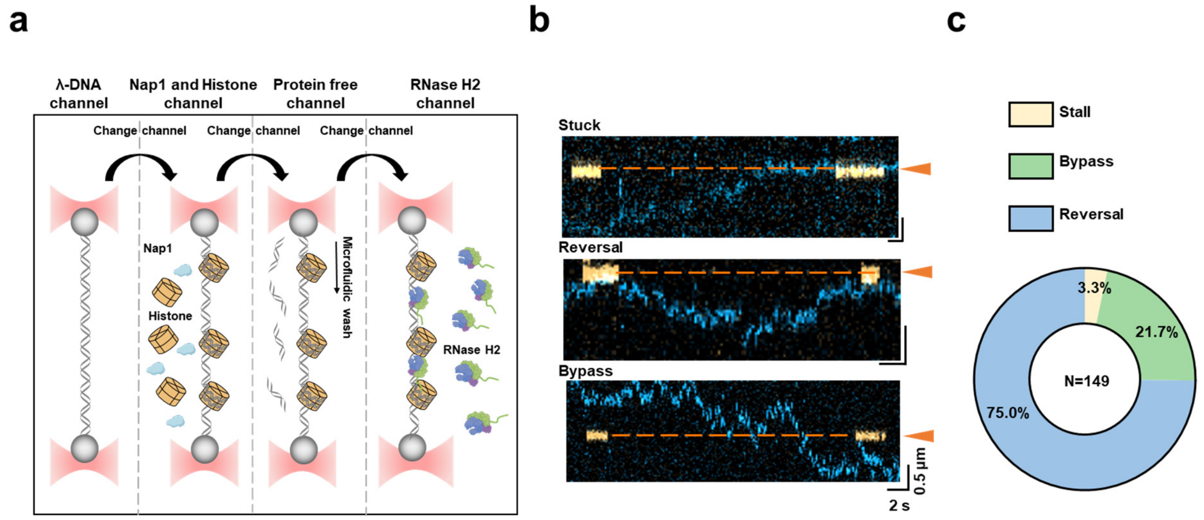

Figure S3. Consequences of the collision between a diffusing RNase H2 and a nucleosome. (a) Workflow for in situ nucleosome assembly and RNase H2 loading. Following the capture of a single λ DNA molecule, it was transferred into a channel containing Nap1 and core histones to initiate nucleosome assembly. The DNA-histone complexes were maintained under sub-piconewton mechanical tension until discrete fluorescent foci emerged. The DNA tether was then transferred to a chamber containing a competitive binding agent to displace non-specifically bound proteins. This was followed by a precisely controlled microfluidic wash to remove unbound histones and Nap1, thereby purifying the reconstituted nucleoprotein complexes. Finally, the nucleosomal λ DNA was transferred to the RNase H2 channel for subsequent functional assays. **(b)** Upon encountering a nucleosome, RNase H2 exhibits diverse characteristic outcomes, including stall, reversal, or bypass. The orange arrow indicates nucleosome position. A brief 640 nm laser pulse was applied to confirm the presence of the nucleosome. The yellow triangles indicate the positions of nucleosomes. **(c)** Pie chart showing the distribution of the indicated outcomes.

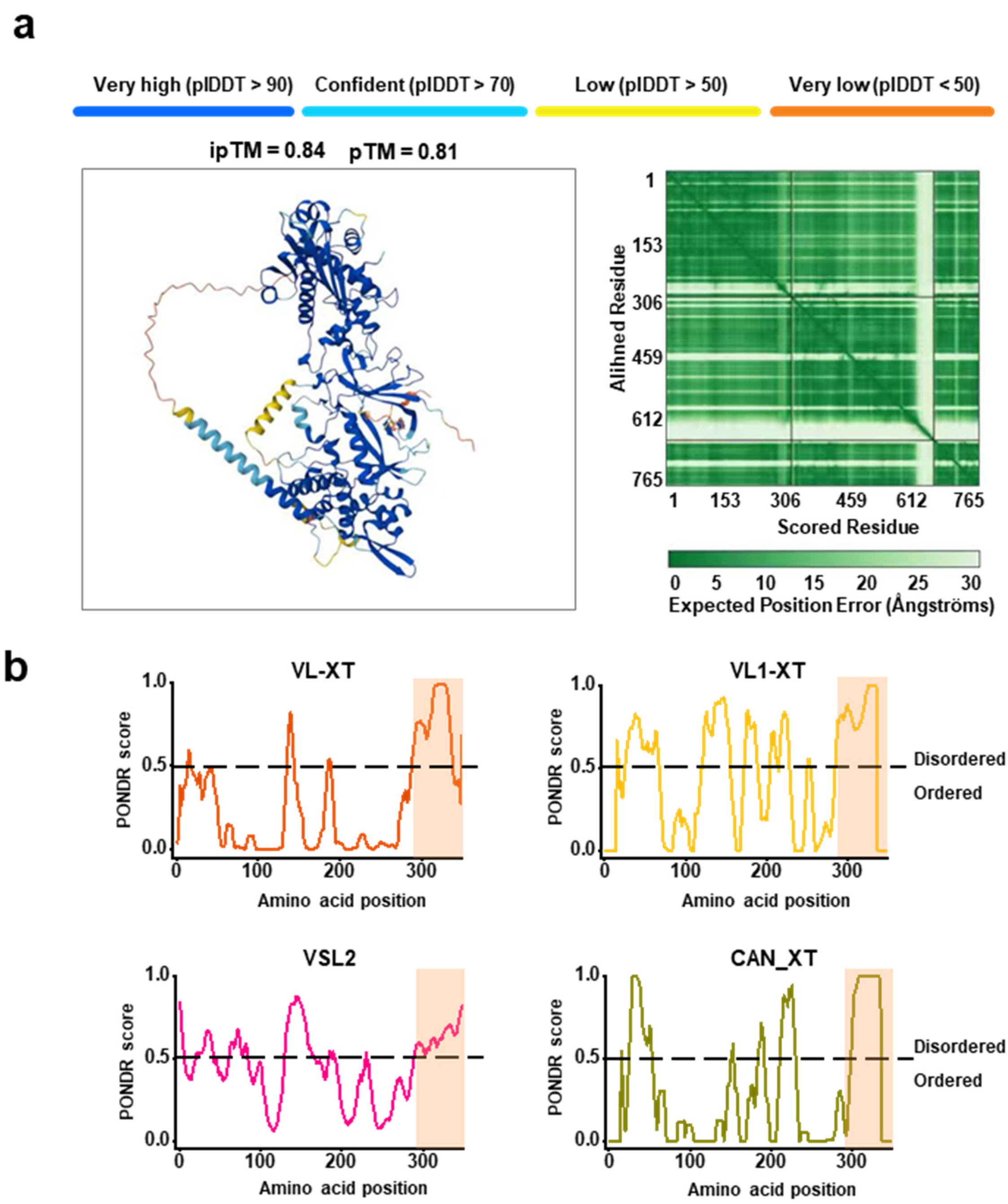

Figure S4. Prediction of the RNase H2 IDR. (a) protein structure prediction of RNase H2 by AlphaFold3. On the right, the AlphaFold Predicted Aligned Error (PAE) heatmap displays the distance error for each pair of residues, which estimates the positional uncertainty of residues in the predicted structure shown[1]. **(b)** The PONDR disorder score for the Rnh202 subunit was predicted by multiple computational models.

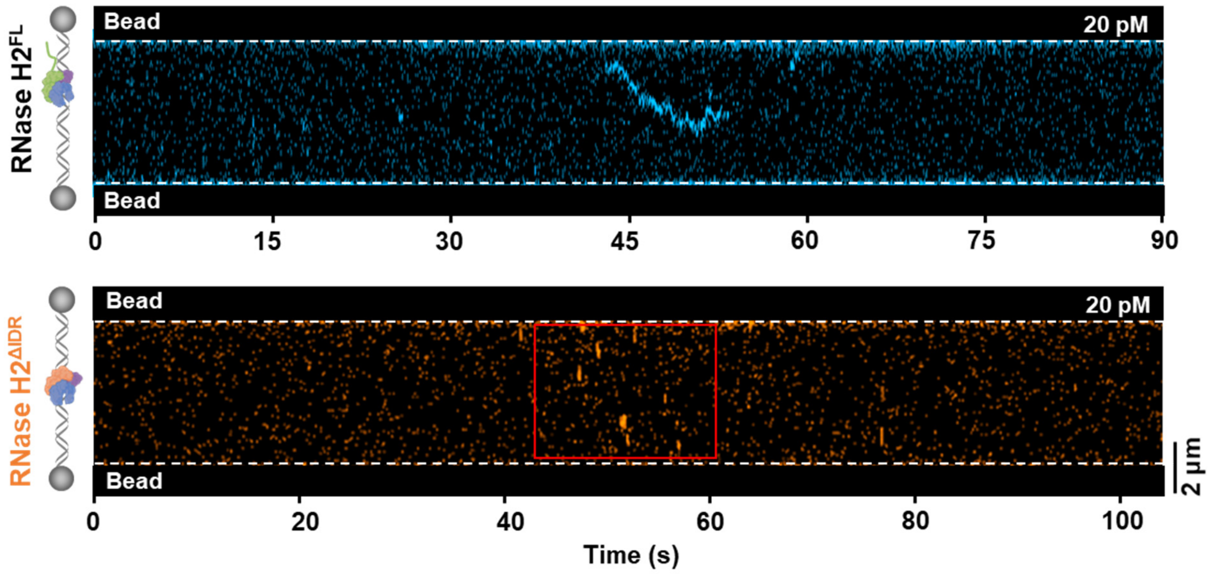

Figure S5. DNA-binding characteristics of RNase H2^{FL} and RNase H2$^{\Delta IDR}$ at an extremely low concentration. Representative kymographs show the binding of RNase H2^{FL}-eGFP and RNase H2$^{\Delta IDR}$-eGFP to 20-kbp naked DNA at a low protein concentration (20 pM). RNase H2^{FL} typically displayed a single, long-lived diffusion event throughout extended observation periods. In contrast, RNase H2$^{\Delta IDR}$ not only exhibited a prolonged lag time prior to the initial binding event but also subsequently generated a burst of short-lived binding events within a narrow time window, as indicated in the red rectangle.

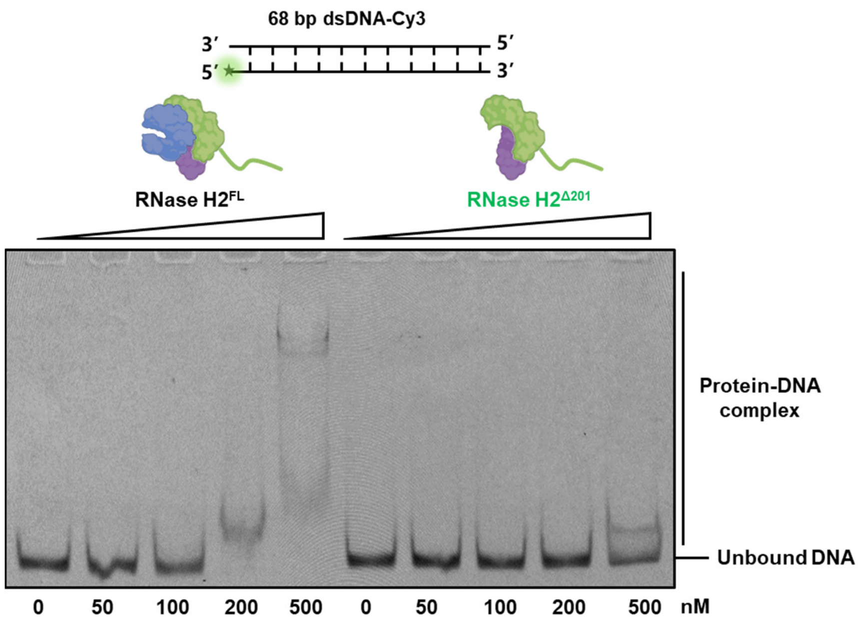

Figure S6. Comparison of RNase H2^{FL} and RNase H2$^{\Delta 201}$ binding to DNA by EMSA. A representative Electrophoretic Mobility Shift Assay (EMSA) gel demonstrates that RNase H2^{FL} possesses a stronger binding affinity for dsDNA compared to the RNase H2$^{\Delta 201}$ variant. Specifically, EMSAs were performed using a Cy3-labeled 68-bp dsDNA substrate **(Table S1)**. A constant concentration of 10 nM dsDNA was mixed with an equal volume of RNase H2^{FL} or RNase H2$^{\Delta 201}$ at final concentrations of 50, 100, 200, or 500 nM in reaction buffer containing 25 mM Tris-HCl (pH 8.0), 50 mM KCl, 2 mM $CaCl_2$, 0.1 mg/mL BSA, and 1 mM DTT. The reaction mixtures were incubated at 37 °C for 15 min. Following that, the samples were supplemented with 50% glycerol and resolved on native 8% polyacrylamide gels. Electrophoresis was carried out at 140 V for 45 min at room temperature using 0.5× TBE running buffer. Gels were visualized using a Typhoon 9500 imager (GE Healthcare) with a 532 nm laser.

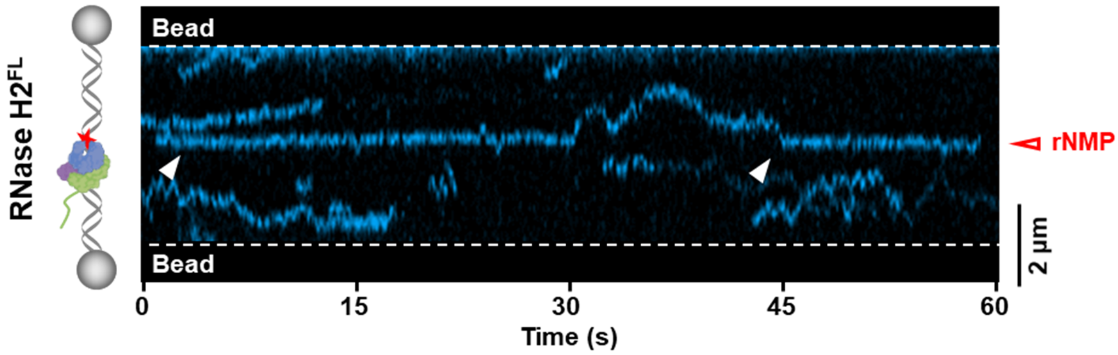

Figure S7. RNase H2 continuously diffuses after 1D targeting an rNMP site. A representative kymograph shows that RNase H2 pauses at the rNMP site for tens of seconds before resuming diffusion. A red arrow marks the rNMP position; white arrows indicate successful recognition events.

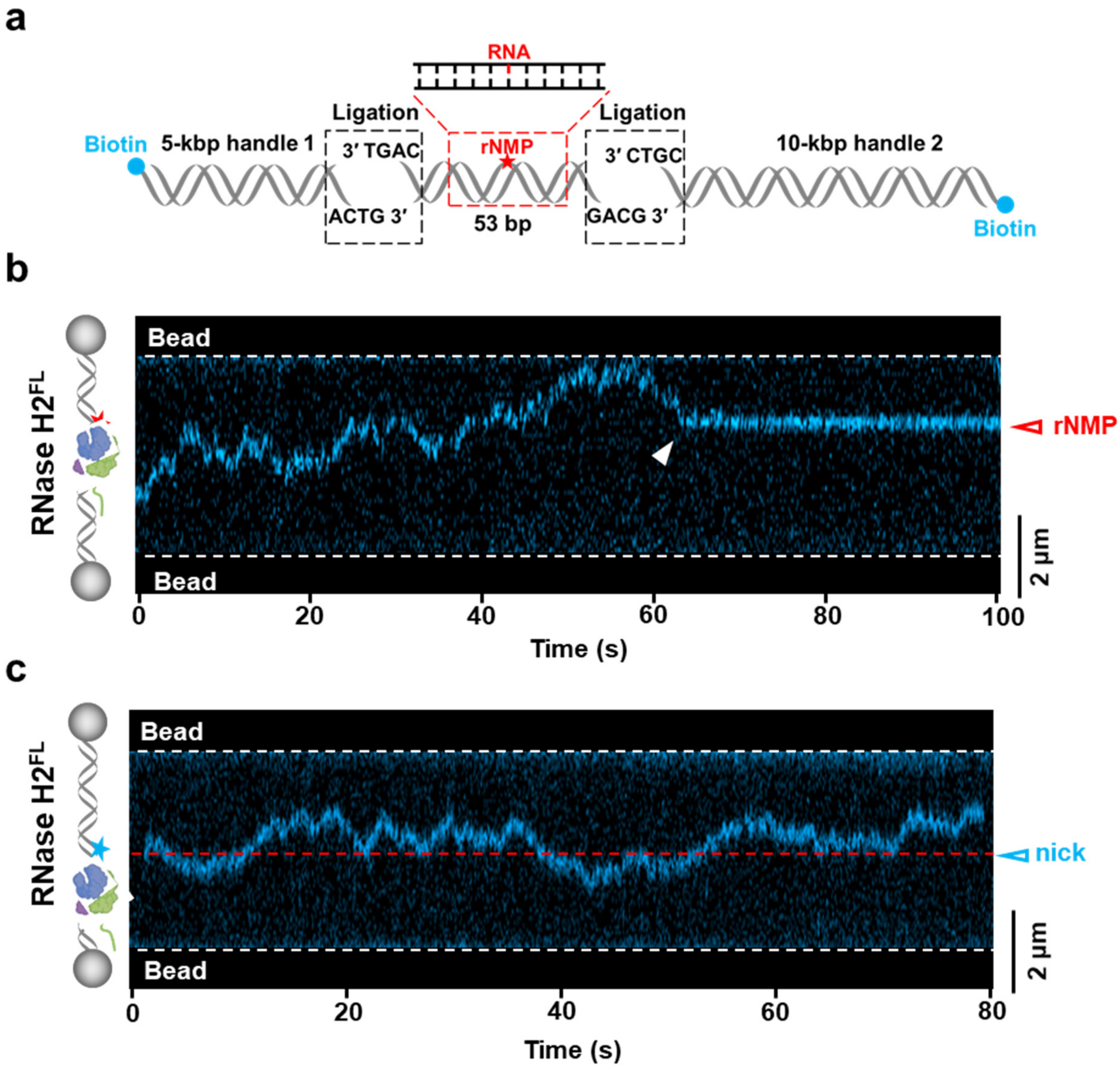

Figure S8. Diffusing RNase H2 stalls because of embedded rNMPs, not DNA nicks. **(a)** Schematic of the construction of the 15-kbp DRD/D construct. A 53-bp duplex containing a single rNMP (red star) connects a 10-kbp handle and a 5-kbp handle via ligation to construct the rNMP-containing substrate. **(b)** A representative kymograph showing RNase H2 successfully locating an rNMP site at the one-third position of a 15-kbp DNA molecule. A red arrow marks the rNMP position; a white arrow indicates a successful recognition event. **(c)** A representative kymograph demonstrating that RNase H2 repeatedly bypasses a nick site without recognition or stable binding. Up to 96% of traversing RNase H2 bypassed the nick site (N=82). A blue arrow marks the nick position.

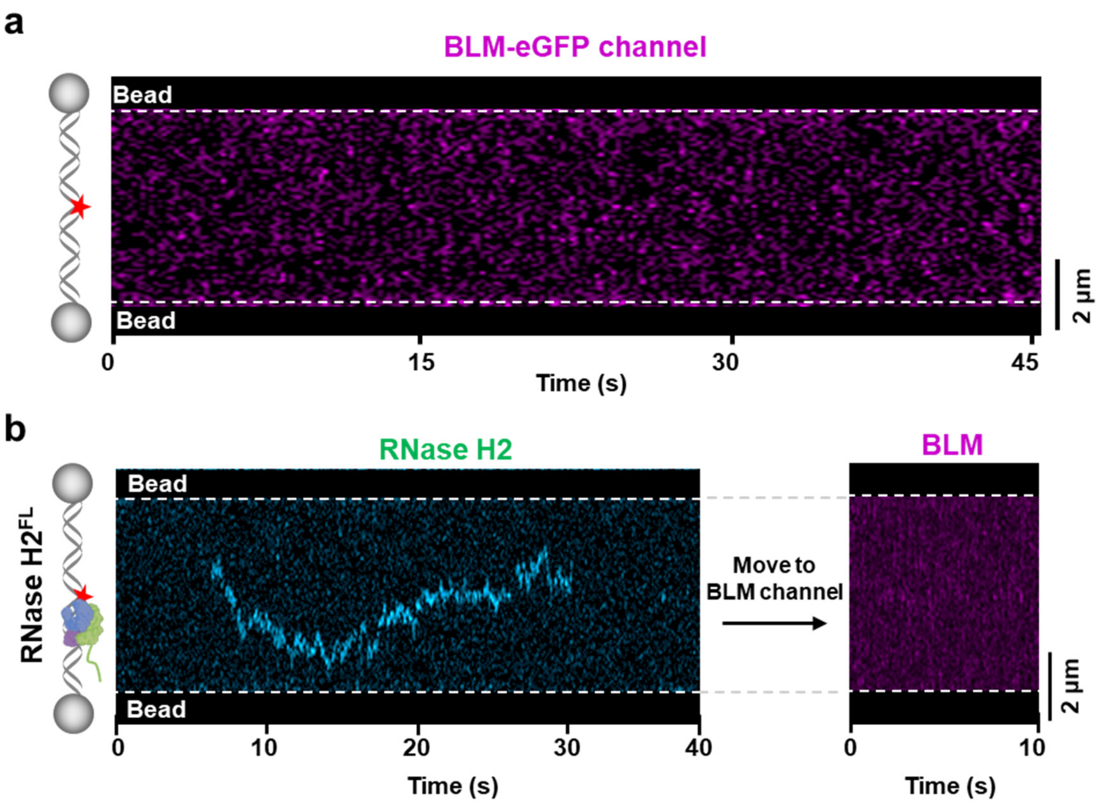

Figure S9. Nick incision by RNase H2^{FL} causes BLM binding. (a) A representative kymograph excluding the possibility of BLM specific binding to rNMP sites. **(b)** Representative kymographs confirming that BLM recruitment depends on RNase H2^{FL} activity. No site-specific binding was observed for BLM, even if RNase H2 passed through the rNMP site without incision.

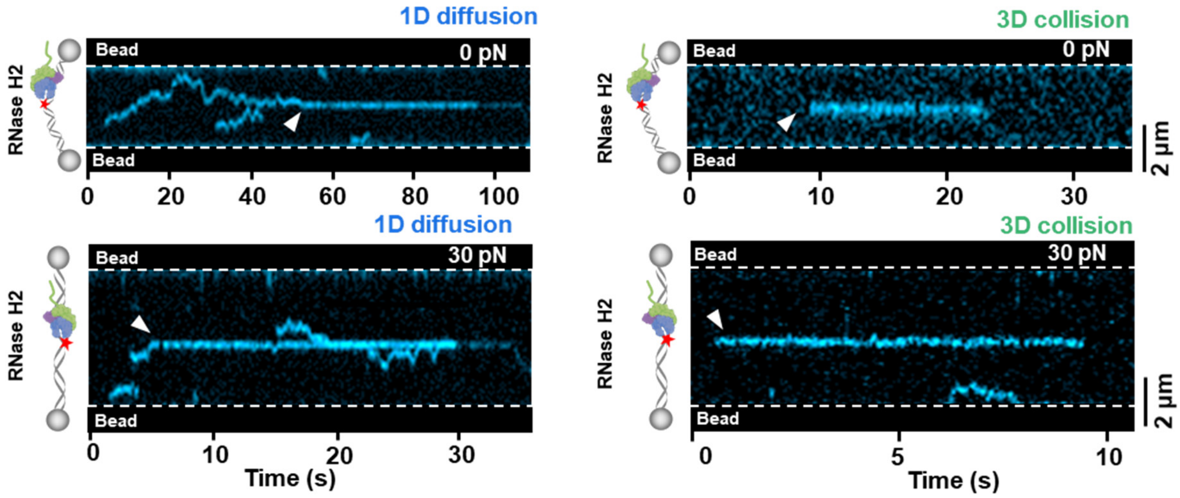

Figure S10. RNase H2 employs two pathways to search for rNMP sites under varying force. Representative kymographs illustrating 1D diffusion and 3D collision target search modes employed by RNase H2 to target the rNMP site in DNA under ~ 0 pN and 30 pN tension. Red arrows indicate the position of the rNMPs. White arrows indicate successful recognition events.

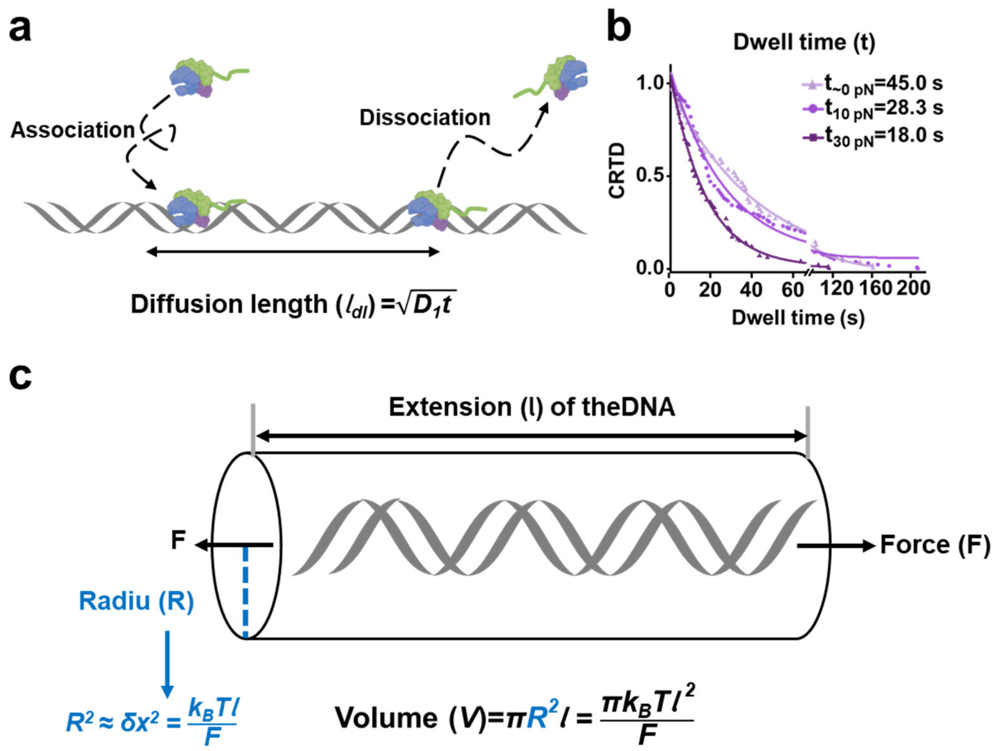

Figure S11. Calculation of RNase H2 diffusion length and the confined volume of the suspended DNA. (a) The schematic illustrates the method for calculating the diffusion length (l_{dl}). $l_{dl}=\sqrt{D_1 t}$, where D_1 denotes the 1D diffusion coefficient of the protein on DNA, and t represents its dwell time[2]. **(b)** CRTD analysis of RNase H2 bound at a nonspecific site under different forces. CRTDs were fit with a one-phase decay model to extract dwell times. Data are from N = 56 (~0 pN), 134 (10 pN), and 100 (30 pN) independent binding events. **(c)** When estimating the equivalent volume of DNA under different stretching forces, we simplify it as a cylindrical model. The radius of the cylinder is derived from the thermodynamic relationship between transverse Brownian fluctuations and the applied stretching force, based on the following expression: $R^2 \approx \delta x^2 = \frac{k_B T l}{F}$. Here, R represents the equivalent cylindrical radius, whose square approximates the mean-square displacement δx^2 of the magnetic bead in the transverse direction, k_B is the Boltzmann constant, T is the temperature, l is the extension of the DNA, and F is the applied stretching force[3].

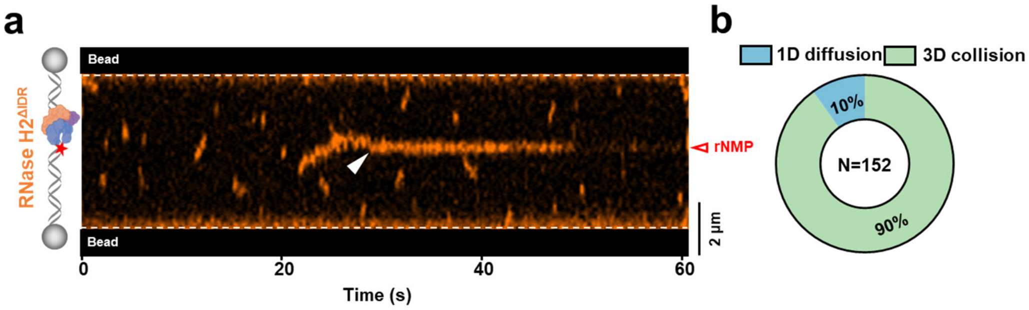

Figure S12.The rare detected 1D rNMP search of RNase H2$^{\Delta IDR}$. (a) A representative kymograph showing RNase H2$^{\Delta IDR}$ targets rNMP site through 1D diffusion. A red arrow marks the rNMP position; a white arrow indicates a successful recognition event. **(b)** Quantification of the percentage of target search events mediated by 1D versus 3D collision for RNase H2$^{\Delta IDR}$.

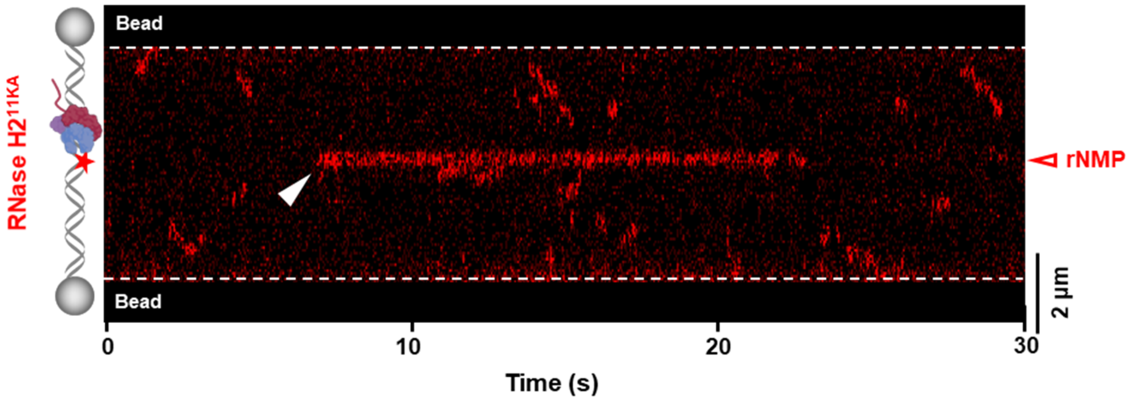

Figure S13. RNase H2^{11KA} searches for rNMP by 3D collision. A representative kymograph showing 3D collision-directed rNMP targeting by RNase H2^{11KA}. A red arrow indicates the position of the rNMP. A red arrow marks the rNMP position; a white arrow indicates a successful recognition event.

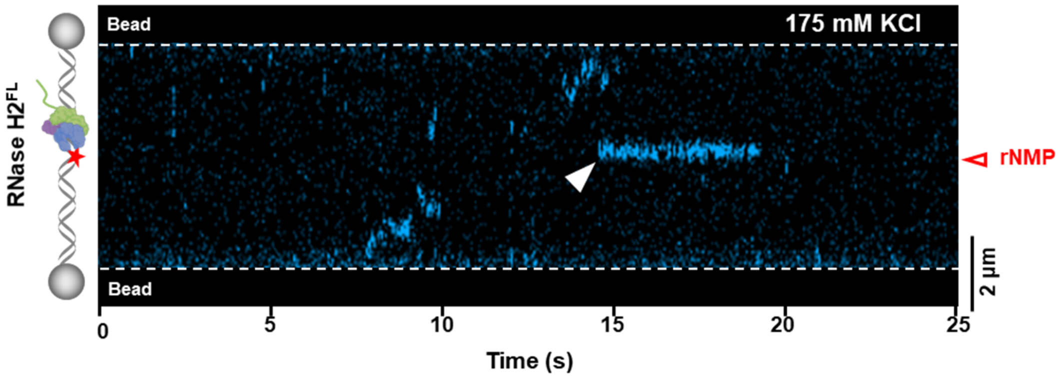

Figure S14. RNase H2^{FL} searches for rNMP by 3D collision under high salt. A representative kymograph showing 3D diffusion-directed rNMP targeting by RNase H2 under a high-salt condition (175 mM KCl). A red arrow indicates the position of the rNMP. A red arrow marks the rNMP position; a white arrow indicates a successful recognition event.

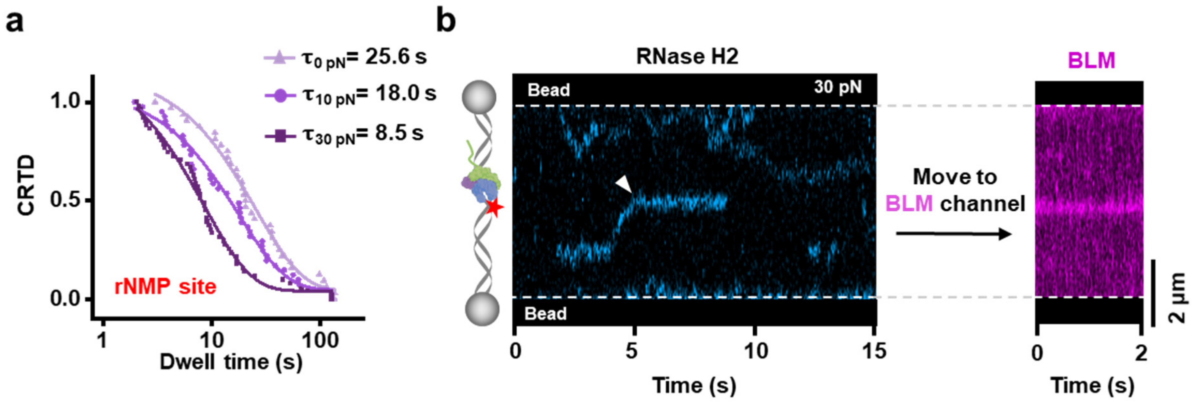

Figure S15. RNase H2 incises rNMPs under high tension. (a) CRTD analysis of RNase H2 bound at rNMP site under different forces. CRTDs were fit with a one-phase decay model to extract dwell times. **(b)** Representative kymographs showing that BLM binds to the rNMPs, indicating that under 30 pN, RNase H2 also incises after recognizing rNMP sites. A white arrow indicates a successful recognition event.

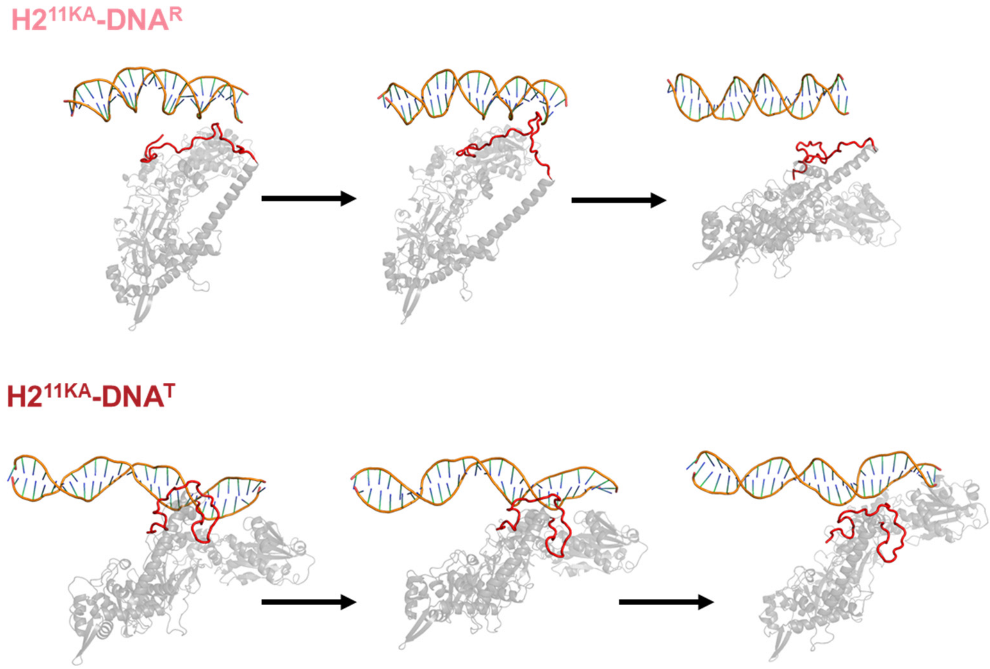

Figure S16. Interactions between the RNase H2^{11KA} IDR and DNA$^{R/T}$ unveiled by MD simulations. Representative structural snapshots of the interaction interface between the RNase H2^{11KA} IDR and relaxed versus tensioned DNA. Unlike RNase H2^{FL}, the charge-neutralized RNase H2^{11KA} exhibits negligible physical contacts, hydrogen bonds, and interaction energies with DNA substrates. RNase H2^{11KA} detachment from DNA was explicitly captured in multiple independent trajectories, indicating a near-complete loss of electrostatic tethering and explaining the abolished mechanosensing capability in this variant.

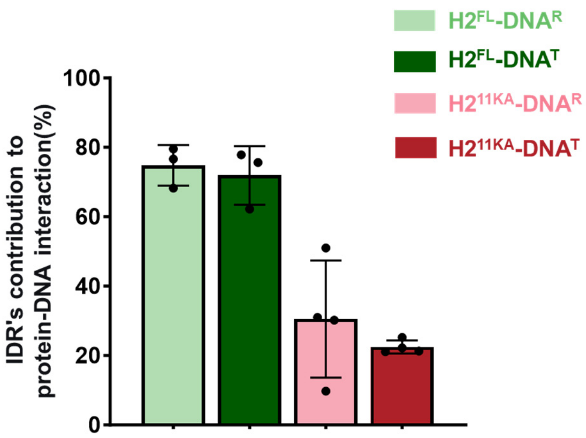

Figure S17. The contribution of IDR to the overall RNase H2–DNA interactions. The bar graph illustrates the contribution of the IDR to the total RNase H2–DNA binding energy. For RNase H2^{FL}, the IDR contributes approximately 70–75% of the total binding energy (primarily through Coulombic interactions), whereas this contribution drops to approximately 25–30% for the RNase H2^{11KA} variant. Data represent mean ± SD from three or four independent simulation trajectories.

Supplementary Table S1. The sequences of primers and oligonucleotides used.

Template	Name	Sequence
Primes for handles	10-kbp handle 1	5′-CTGCAGAACCATCAGTATGGTATATTGTAAAGCTGAGTATTGGTTTATTTGGCG-3′
		5′-biotin-TGATAAGCAGAATGGCATCGTTCC-3′
	10-kbp handle 2	5′-CTGCAGAACCATGACGATGGTATTAAAGCTGAGTATTGGTTTATTTGGCG-3′
		5′-biotin-TGATAAGCAGAATGGCATCGTTCC-3′
	5-kbp handle 1	5′-CTGCAGAACCATCAGTATGGGCATATGTTGTGTTTTACAGTATTATGTAGTCTGTTT-3′
		5′-biotin-TGATAAGCAGAATGGCATCGTTCC-3′
53 bp intact DNA	Upper	5′P-GCTGAGCAATCAGGATTGCAATCATGGTTCCTGCATTAGCTCGACAGGTCAGT-3′
	Lower	5′P-CCTGTCGAGCTAATGCAGGAACCATGATTGCAATCCTGATTGCTCAGCGACG-3′
53 bp nicked DNA	Upper 1	5′P-GCTGAGCAATCAGGATTGCAATCATGGTTCCTGCATT-3′
	Upper 2	5′P-AGCTCGACAGGTCAGT-3′
	Lower	5′P-CCTGTCGAGCTAATGCAGGAACCATGATTGCAATCCTGATTGCTCAGCGACG-3′
53 bp DRD/D	Upper-R	5′P-GCTGAGCAATCAGGATTGCAATCATGGTTCCTGCAT/rU/AGCTCGACAGGTCAGT-3′
	Lower	5′P-CCTGTCGAGCTAATGCAGGAACCATGATTGCAATCCTGATTGCTCAGCGACG-3′
53 bp DRD/D-FAM	Upper-R-FAM	5′FAM-GCTGAGCAATCAGGATTGCAATCATGGTTCCTGCAT/rU/AGCTCGACAGGTCAGT-3′
	Lower	5′P-CCTGTCGAGCTAATGCAGGAACCATGATTGCAATCCTGATTGCTCAGCGACG-3′
68 bp DNA-Cy3	Upper-Cy3	5′Cy3-TCAACCCGATGTTTGAGTACGGTCATCATCTGACACTACAGACTCTGGCATCGCTGTGAAGACGACGC-3′
	Lower	5′GCGTCGTCTTCACAGCGATGCCAGAGTCTGTAGTGTCAGATGATGACCGTACTCAAACATCGGGTTGA-3′

The rNMPs are colored red.

Supplementary References

1. Abramson, J. et al. Addendum: Accurate structure prediction of biomolecular interactions with AlphaFold 3. Nature 636, 493-500 (2024).
2. Halford, S.E. & Marko, J.F. How do site-specific DNA-binding proteins find their targets? Nucleic Acids Res 32, 3040-3052 (2004).
3. Strick, T.R., Allemand, J.F., Bensimon, D. & Croquette, V. Behavior of supercoiled DNA. Biophys J 74, 2016-2028 (1998).